Composition and formation age of the amorphous silica coating glacially polished surfaces

Terrence Blackburn[1], Shalev Siman-Tov[2], Matthew A. Coble[3], Greg M. Stock[4], Emily E. Brodsky[1], Bernard Hallet[5]

[1] *University of California Santa Cruz, CA, USA*

[2] *Geological Survey of Israel, Jerusalem, Israel*

[3] *Stanford University, Stanford, CA, USA*

[4] *National Park Service, Yosemite National Park, El Portal, CA, USA*

[5] *University of Washington, Seattle, WA, USA*

ABSTRACT

Recent micrographs of smooth, glacially abraded silicic bedrock reveal an amorphous coating layer adhering to the bedrock, with structures that tie its formation to glacial abrasion. What remains unclear is whether this coating is formed by the physical comminution of bedrock, resulting in amorphous material with a bedrock composition, or by chemical dissolution of silicate minerals followed by precipitation of an amorphous layer enriched in silica and depleted in cations relative to the bedrock. Here we report the composition and formation age of the amorphous coatings in Yosemite National Park, California. The coatings are depleted in base cations (50-90%) and enriched in silica (10-50%) as well as trace Fe and U (4-100-fold) relative to the bedrock, reflecting dissolution by and precipitation from subglacial waters. The $^{234}U/^{238}U$ activity ratio of the amorphous layer is 200-600% above secular equilibrium, reflecting a surficial U-source enriched by α-recoil processes and consistent with the ^{234}U enrichment

observed in subglacial waters. The $^{230}Th/^{238}U$ activity ratio is 30-100% below secular equilibrium and records thorium-uranium fractionation in subglacial waters at 10-30 ka, consistent with coating formation during the Last Glacial Maximum (LGM). These amorphous coatings are subglacial precipitates that record the chemical weathering of silicates beneath glaciers during the LGM. Collectively, these observations link silicate dissolution and amorphous silica production to physical processes at the glacier bed, a result that may well have significant implications for the global Si and CO_2 budgets on glacial-interglacial timescales.

INTRODUCTION

Glaciers are renowned for their ability to physically erode landscapes. This physical erosion occurs beneath glacial ice through sliding at the base of warm-based glaciers by both quarrying and abrasion of bedrock, which produces large volumes of glacial silt and clay-sized particles. Particle comminution greatly increases the surface area of minerals on which chemical weathering can operate, a process that has been inferred to increase chemical denudation rates above average rates for non-glaciated catchments (Anderson et al., 1997). The composition of subglacial water is distinct from those of non-glaciated catchments and reflects a unique chemical weathering regime beneath glaciers (Anderson et al., 1997; Torres et al., 2017).

How glaciers chemically interact with the continental crust globally, and the types of weathering reactions that occur, are fundamental to understanding whether glaciers operate as a net CO_2 source or sink. This balance ultimately determines the feedbacks between glacial processes and Earth's climate over interglacial-glacial cycles. In studies of modern alpine glaciers, the most abundant solutes in glacial runoff, Ca^{2+} and HCO_3^- and SO_4^{2-} (e.g. Sharp et al., 1995; Torres et al., 2017) have led to the interpretation that the primary chemical weathering reaction beneath glaciers is the dissolution of carbonates and oxidation of sulfides, a result that holds even though calcite and pyrite are found only in trace abundances in granitic or gneissic catchments (Erel et al., 2004). If the extent of chemical weathering beneath glaciers is indeed limited to reactions with trace carbonate and sulfate, phases that release CO_2 upon dissolving, glaciers are a source of CO_2 and potentially buffer the net cooling that occurs during glacial intervals (Sharp et al., 1995; Torres et al., 2017). Reactions such as the dissolution of silicates would have the opposite effect, releasing both Si and alkaline metals, the former drawing down CO_2 during diatom blooms on shorter timescales, whereas the latter may contribute to carbonate formation and CO_2 sequestration on longer timescales (Graly et al., 2017). Yet the degree to which silicate weathering occurs beneath glaciers has, based on low dissolved Si concentration in glacial runoff, previously been regarded as highly limited (Anderson et al., 1997; Torres et al., 2017).

Emerging data suggest that these observations collected from modern alpine glaciers may not apply to all subglacial settings. Beneath Greenland ice masses, for example, glacial waters can indeed carry significant loads of Si to global oceans, in the form of undissolved amorphous Si grains suspended within turbid glacial runoff, which dissolve upon reaching the saline ocean (Hawkings et al., 2017). Though there is at present no known connection between the formation of these amorphous grains and any specific glacial process, this observation hints that any chemical interaction between glaciers and the siliceous continental crust may be underestimated by a factor of 10 (Hawkings et al., 2017; Torres et al., 2017).

One place to examine the chemical interaction between glacial ice and silicate crust is where rocky outcrops have been eroded and polished by glacial action to a smooth, glossy bedrock surface known as glacial polish. It has been commonly assumed that these mirror-like surfaces are generated by the mechanical process of abrasion during which basal debris-rich ice and rock removes protrusions until a surface is optically smooth (Iverson, 1991). A recent investigation by Siman-Tov and others (2017) of glaciated crystalline rocks, however, identified a ~1-4 μm thick layer of predominantly amorphous material supporting sub-micron mineral fragments, collectively coating the abraded bedrock. This coating was interpreted to record polish formation by a combination of abrasion, removal, and adhesion of mechanically abraded host rock, ground to submicron mineral fragments, and non-crystalline amorphous material that are spread over the overlying host rock. Though mechanical processes alone could reduce grain size, yielding amorphous material, as observed in experimental granite gouge (Yund et al., 1990), the amorphous coatings on silicate rock can also occur as a result of chemical weathering, specifically the dissolution of silicates and reprecipitation amorphous silica. In experimental studies, nanometer thick layers (< 0.1 μm) of hydrated silica form upon silicates from exposure to fluids (Hellmann et al., 2012). These layers are chemically distinct, with high total silica and low base cations relative to the underlying host mineral. If the amorphous material occurring on glacially polished surfaces exhibits similar compositional traits, it suggests: 1) a significant role of chemical weathering in polish formation; 2) a likely mechanism for the formation of amorphous silica particles in glacial runoff, which are also found to be enriched in Si and depleted in cations (Hawkings et al., 2017), and 3) a previously unrecognized archive of former glacier sliding and silicate chemical weathering occurring beneath glaciers that has implications for the global Si and CO_2 budgets.

METHODS & RESULTS

Here we present the results of a geochemical and isotopic investigation that utilized *in-situ* analytical techniques (LA-ICPMS and SHRIMP-RG) to determine the major, trace, and U-series isotopic composition of the microns thick amorphous layer within glacially polished surfaces collected from Yosemite National Park, California (Appendix DR1). Samples were collected from Lyell Canyon and Tuolumne Meadows, areas dominated by crystalline granodiorite that deglaciated ~10-15 ka (Dühnforth et al., 2010) ago at the end of the Last Glacial Maximum. In a prior study, these samples were the focus of a microstructural investigation using TEM imaging (Siman-Tov et al., 2017) that complements and provides a visual reference to the new geochemical data presented below.

The composition of the glacial polish layer

The composition of the glacial polish layer was determined using the UCSC LA-ICPMS system (see Appendix DR2 for methods). A single laser spot analysis collected from Daff Dome (Daff01) in Tuolumne Meadows provides a representative example of a continuous major and trace elemental profile from the polish surface down into the underlying bedrock. In the example shown in Figure 1A, the mineral grain beneath the polish is plagioclase feldspar with high Si, Al, Na, and Ca, but also with detectable K, Fe, Mg. U and Th concentrations are < 5 ppm. Approximately 3 μm below the coating surface, the abundances of all measured elements change. The total silica increases toward the surface, while concentrations of base cations abundant in the underlying mineral (Na, Ca) decrease. Cations not abundant in host plagioclase (K, Mg, Fe, U, Th), are found at higher concentrations near the surface. Comparison to TEM images from a nearby plagioclase grain (Fig. 1B) reveals a plagioclase capped by a ~3 μm thick layer of predominantly amorphous material supporting loosely aligned, sub-micron fragments of mostly quartz, plagioclase and alkali feldspars, as well as Fe oxides.

Multiple laser spot analyses collected from a centimeter-sized glacial polish sample from Daff Dome (Daff01) reveal compositional changes above each rock-forming mineral within the bedrock. A comparison of cation to SiO_2 concentrations for all spot analyses, color coded by ablation depth, permits identification of: 1) the composition of the underlying bedrock minerals (Fig. 2 yellow) and; 2) the composition of the polish layer (Fig. 2 green & blue). Na_2O at >3µm depths (Fig. 2A, yellow), for example, reveals bedrock minerals beneath the polish layer of both Na- enriched and depleted feldspars (~65% SiO_2) along with quartz (~100% SiO_2). At shallow depths (Fig. 2, blue) the composition is relatively uniform (~70-80 wt% SiO_2, ~1 wt% Na_2O) for the polish layer, independent of the underlying mineral. This observation extends to all measured major elements, suggesting that the polish occupies a relatively narrow compositional space that is distinct from all of the underlying minerals (Fig. 2 A-F).

To determine what chemical processes are operating to generate the glacial polish layer, we define the polish composition using a cluster analysis for each laser ablation spot analysis and compare it to the bulk composition of the underlying host rock. Polish compositions for each laser spot are shown as red circles for Daff Dome (Fig. 2) and five additional samples from Lyell Canyon (see Appendix DR2). Comparison between polish and bedrock compositions reveals compositional trends that include the enrichment in Si by up to 30 wt% relative to the whole rock values (Fig. 3). This Si enrichment is coupled with loss of 50-90% of Na, K, Mg, and Ca relative to bulk bedrock compositions (Fig. 3A-D). In contrast, Uranium can be enriched in some locations up to 100-fold relative to the bedrock (Fig. 3F).

Subglacial processes and the formation age of the glacial polish layer

The U-series decay chain members such as ^{234}U and ^{230}Th can, by chemical or physical processes, be enriched or depleted relative to parent ^{238}U. Fractionation of these "intermediate daughters" can be utilized to measure geologic time and/or reflect the formation environment. U-series (^{230}Th-^{232}Th-^{234}U-^{238}U) determinations of the glacially polished surface from Daff Dome (Daff01) were collected using the SHRIMP-RG ion microprobe. See Appendix DR3 for methods and data table. Multiple spot analyses all occupy a distinct isotopic space where $^{234}U/^{238}U$ activity ratios are 200-600% above secular equilibrium, whereas the $^{230}Th/^{238}U$ activity ratios are 30-100% below. These isotopic compositions can be bracketed by isochronous curves that place ^{230}Th fractionation from ^{234}U over a range of timescales from ~10 to 30 ka (Fig. 4).

DISCUSSION

The Formation of the Amorphous Layer

The compositional comparison of the polish layer and underlying bedrock suggests that the amorphous layer is not directly related to the underlying bedrock (Fig. 1). Rather, the amorphous layer occupies a relatively narrow compositional space, distinct from all underlying minerals (Fig. 2), with compositional variability likely attributed to mineral fragments within the layer (e.g. Fig 1B). Next, the loss of nearly all cations coupled with an increase in SiO_2 (Fig. 3) corresponding to depths imaged as structurally amorphous (Fig 1B) is consistent with silicate dissolution at the fluid-rock interface followed by the precipitation of amorphous silica from subglacial water (Hallet, 1975; Hellmann et al., 2012; Rutledge et al., 2018).

The role of subglacial fluids is further supported by the high concentrations of uranium in the polish relative to the bedrock, an observation that requires sourcing outside of the bedrock.

This hypothesis is supported by the high $^{234}U/^{238}U$ in the amorphous layer (Fig. 4), an observation that indicates a surficial, non-bedrock U-source where ^{234}U is enriched by the physical fractionation from ^{238}U. The high-energy α-decay of parent ^{238}U housed within silicates, results in the ejection of ^{234}U from fine-grained sediments into subglacial fluids or ice. Elevated $^{234}U/^{238}U$ values have been observed in glacial runoff (Arendt et al., 2018; von Strandmann et al., 2006) and reflect interaction between rock and ice. A subglacial water source is also supported by the ^{230}Th-U data, which suggests, that insoluble ^{230}Th was absent from subglacial waters relative to fluid-mobile U. The isotopic space defined by the amorphous layer records chemical fractionation in subglacial fluids occurring over 10 to 30 ka, consistent with the formation of amorphous material over a time range spanning the Last Glacial Maximum (Clark et al., 2009) to deglaciation in Yosemite (Dühnforth et al., 2010).

Collectively, we interpret the compositional and isotopic data presented here to record the subglacial dissolution of silicate rock and production of amorphous silica during the LGM. We propose that glacial action comminutes particles at the ice-rock interface, increasing the surface area of silicate wear particles. Glacial sliding is one possible driver for chemical activity at the glacier bed; local pressure melting in high pressure areas produce undersaturated subglacial waters which can dissolve minerals, while local freezing in low pressure areas can consume subglacial water, concentrating solutes to the point of precipitation (Hallet, 1975). Base cations (Na, K, Mg, Ca) largely remain within subglacial waters, while amorphous Si is precipitated, incorporating Fe, U and the U-series composition of subglacial waters.

Potential implications for global element cycles

The compositional data and direct images from the glacial polish layer produced at the ice-rock interface suggest a likely location for the generation of amorphous silica grains and coatings to particles observed within glacial runoff (Hawkings et al., 2017). Such a mechanism is of special interest because enhanced Si delivery to the oceans during glacial intervals could produce diatom blooms, previously hypothesized to account for decreased atmospheric CO_2 during glacial periods (Harrison, 2000), which is consistent with both low Ge/Si values in marine opals (Froelich et al., 1992) and higher Si concentrations in marine sponges (Jochum et al., 2017) formed during glacial intervals. Finally, the data presented here shows that the generation of amorphous silica must include the delivery of alkaline metals (e.g. Ca^{2+}, Mg^{2+}) to global oceans, a reaction that could sequester CO_2 on longer timescales should these contributions outweigh subaerial ones.

CONCLUSIONS

We interpret the compositional and isotopic data presented here to record the subglacial dissolution of silicate rock and production of amorphous silica beneath glaciers in the Sierra Nevada, California, during the Last Glacial Maximum. Glacial polish, a ubiquitous feature of glaciated landscapes, is now recognized as being constructed of subglacial chemical precipitates that archive the composition of subglacial waters and permit geochronologic constraints to be placed on the timing of temperate ice cover and subglacial chemical weathering of silicates.

ACKNOWLEDGMENTS

We thank Joseph Graly, Kurt Cuffey and an anonymous reader for their constructive reviews. Thanks also to Rob Franks for assisting in data collection and to Ken Ferrier and Joel Blum for insightful discussions. This work was supported by a UCSC SRG grant to Blackburn and Brodsky.

REFERENCES CITED

Aciego, S., Bourdon, B., Schwander, J., Baur, H., and Forieri, A., 2011, Toward a radiometric ice clock: uranium ages of the Dome C ice core: Quaternary Science Reviews,30, 2389-2397.

Anderson, S., Drever, J. I., and Humphrey, N. F., 1997, Chemical weathering in glacial environments: Geology,25, 399-402.

Arendt, C. A., Aciego, S. M., Sims, K. W. W., Das, S. B., Sheik, C., and Stevenson, E. I., 2018, Influence of glacial meltwater on global seawater δ 234 U: Geochimica et Cosmochimica Acta,225, 102-115.

Bateman, P. C., Chappell, B. W., Kistler, R. W., Peck, D. L., and Busacca, A., 1988, Tuolumne Meadows quadrangle, California; analytic data: USGPO.

Clark, P. U., Dyke, A. s., Shakun, J. D., Carlson, A. E., Clark, J., Wohlfarth, B., Mitrovica, J. X., Hostetler, S. W., and McCabe, A. M., 2009, The Last Glacial Maximum: Science,325, 710-714.

Dühnforth, M., Anderson, R. S., Ward, D., and Stock, G. M., 2010, Bedrock fracture control of glacial erosion processes and rates: Geology,38, 423-426.

Erel, Y., Blum, J. D., Roueff, E., and Ganor, J., 2004, Lead and strontium isotopes as monitors of experimental granitoid mineral dissolution: Geochimica et Cosmochimica Acta,68, 4649-4663.

Froelich, P. N., Blanc, V., Mortlock, R. A., Chillrud, S. N., Dunstan, W., Udomkit, A., and Peng, T. H., 1992, River fluxes of dissolved silica to the ocean were higher during glacials: Ge/Si in diatoms, rivers, and oceans: Paleoceanography and Paleoclimatology,7, 739-767.

Graly, J. A., Drever, J. I., and Humphrey, N. F., 2017, Calculating the balance between atmospheric CO_2 drawdown and organic carbon oxidation in subglacial hydrochemical systems: Global Biogeochemical Cycles,31, 709-727.

Graly, J. A., Humphrey, N. F., Landowski, C. M., and Harper, J. T., 2014, Chemical weathering under the Greenland ice sheet: Geology,42, 551-554.

Gray, W., Glazner, A. F., Coleman, D. S., and Bartley, J. M., 2008, Long-term geochemical variability of the Late Cretaceous Tuolumne intrusive suite, central Sierra Nevada, California: Geological Society, London, Special Publications,304, 183-201.

Hallet, B., 1975, Subglacial silica deposits: Nature,254, 682.

Harrison, K. G., 2000, Role of increased marine silica input on paleo- pCO_2 levels: Paleoceanography,15, 292-298.

Hawkings, J. R., Wadham, J. L., Benning, L. G., Hendry, K. R., Tranter, M., Tedstone, A., Nienow, P., and Raiswell, R., 2017, Ice sheets as a missing source of silica to the polar oceans: Nature communications,8, 14198.

Hellmann, R., Wirth, R., Daval, D., Barnes, J.-P., Penisson, J.-M., Tisserand, D., Epicier, T., Florin, B., and Hervig, R. L., 2012, Unifying natural and laboratory chemical weathering

with interfacial dissolution–reprecipitation: a study based on the nanometer-scale chemistry of fluid–silicate interfaces: Chemical Geology,294, 203-216.
Iverson, N. R., 1991, Morphology of glacial striae: implications for abrasion of glacier beds and fault surfaces: Geological Society of America Bulletin,103, 1308-1316.
Jochum, K. P., Schuessler, J. A., Wang, X. H., Stoll, B., Weis, U., Müller, W. E. G., Haug, G. H., Andreae, M. O., and Froelich, P. N., 2017, Whole-Ocean Changes in Silica and Ge/Si Ratios During the Last Deglacial Deduced From Long-Lived Giant Glass Sponges: Geophysical Research Letters,44, 22.
Rutledge, A. M., Horgan, B. H. N., Havig, J. R., Rampe, E. B., Scudder, N. A., and Hamilton, T. L., 2018, Silica Dissolution and Precipitation in Glaciated Volcanic Environments and Implications for Mars: Geophysical Research Letters,45, 7371-7381.
Sharp, M., Tranter, M., Brown, G. H., and Skidmore, M., 1995, Rates of chemical denudation and CO2 drawdown in a glacier-covered alpine catchment: Geology,23, 61-64.
Siman-Tov, S., Stock, G. M., Brodsky, E. E., and White, J. C., 2017, The coating layer of glacial polish: Geology,45, 987-990.
Torres, M. A., Moosdorf, N., Hartmann, J., Adkins, J. F., and West, A. J., 2017, Glacial weathering, sulfide oxidation, and global carbon cycle feedbacks: Proceedings of the National Academy of Sciences,114, 8716-8721.
von Strandmann, P. A. E. P., Burton, K. W., James, R. H., van Calsteren, P., Gíslason, S. R., and Mokadem, F., 2006, Riverine behaviour of uranium and lithium isotopes in an actively glaciated basaltic terrain: Earth and Planetary Science Letters,251, 134-147.
Yund, R. A., Blanpied, M. L., Tullis, T. E., and Weeks, J. D., 1990, Amorphous material in high strain experimental fault gouges: Journal of Geophysical Research: Solid Earth,95, 15589-15602.

FIGURE CAPTIONS

Figure 1. **A.** Representative LA-ICPMS element profile for Daff Dome. Note the break in scale after 50 ppm and 25 wt%. See appendix DR 4 for depth calibration. The gradual chemical transitions are an artifact of mixing between suspended mineral fragments and variations in polish thickness which can vary by 1-2 μm on horizontal scales less than the 25μm spot size. **B.** TEM image from Daff dome reveal mostly amorphous silica (aSi) supporting fragments of quartz (qtz), Fe-oxide (FeO), illite (ilt), alkali (kfs) and plagioclase (plg) feldspars above the host plagioclase and capped by a layer of phylosilicates (ph). Note the differing vertical scales for **A** and **B**, connected at 3μm by the white dashed arrow.

Figure 2. Harker diagrams displaying multiple laser spot analyses from Daff dome colored by ablation depth. Abbreviations: underlying host mineral (HM) and polish (P). Red open circles are the averaged polish compositions for major elements (A-E) and maximum concentration for uranium (E) identified for each laser spot. These polish compositions (open red circles) are compared to whole rock data in figure 3.

Figure 3. Glacial polish composition for Daff dome (open red circles, Fig. 2) and 5 samples within Lyell Canyon (DR2). In comparison to whole rock values (stars), polish compositions reflect Si (10-50%) enrichment and cation loss (50-90%) relative to whole rock values (stars) Whole rock values from:(Bateman et al., 1988; Gray et al., 2008). Note that Daff dome polish (red circles) should be compared to Cathedral Peak Granodiorite (red star), while all Lyell canyon polish formed upon the Kuna Crest Granodiorite (blue star).

Figure 4. ^{230}Th-^{234}U-^{238}U data for multiple spots (1σ) measured by SHRIMP-RG on U-rich polish from Daff Dome. Standard BZVV is included. Precipitates forming in the absence of ^{230}Th, with a range of $^{234}U/^{238}U$ initial values (e.g. system starts along Y-axis), evolve to the right, as a result of ^{230}Th ingrowth, following the blue curves towards secular equilibrium (solid line).

[1]GSA Data Repository item 201Xxxx, including sample location and compositional data as well as laboratory methodologies, is available online at www.geosociety.org/pubs/ft20XX.htm, or on request from editing@geosociety.org or Documents Secretary, GSA, P.O. Box 9140, Boulder, CO 80301, USA

FIGURE 1:

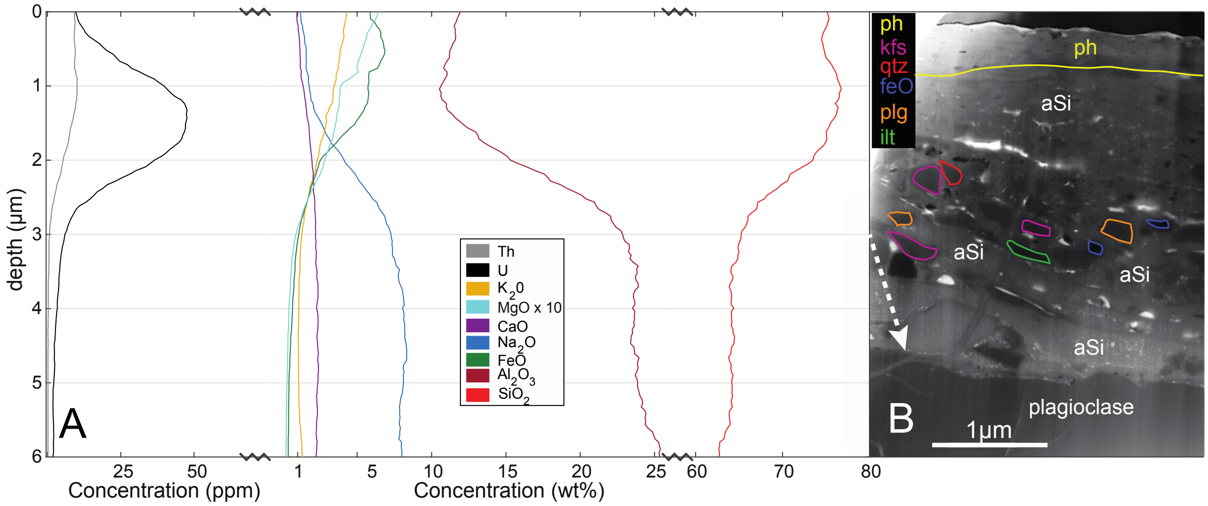
A
depth (µm)
Concentration (ppm)
Concentration (wt%)
Th
U
K2O
MgO x 10
CaO
Na2O
FeO
Al2O3
SiO2
B
ph
kfs
qtz
feO
plg
ilt
aSi
plagioclase
1µm

Figure 2

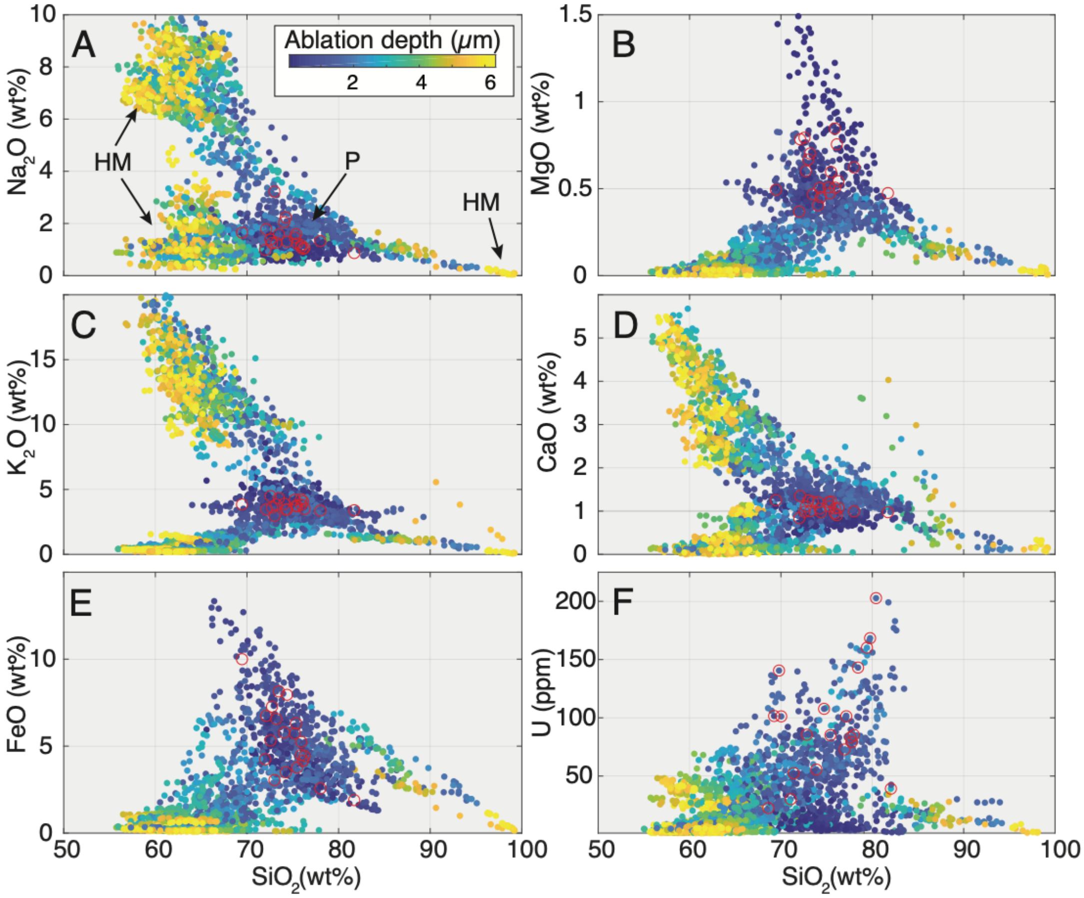
A
B
C
D
E
F
Ablation depth (μm)
2 4 6
HM
HM
P
HM
Na_2O (wt%)
MgO (wt%)
K_2O (wt%)
CaO (wt%)
FeO (wt%)
U (ppm)
SiO_2(wt%)
SiO_2(wt%)

Figure 3

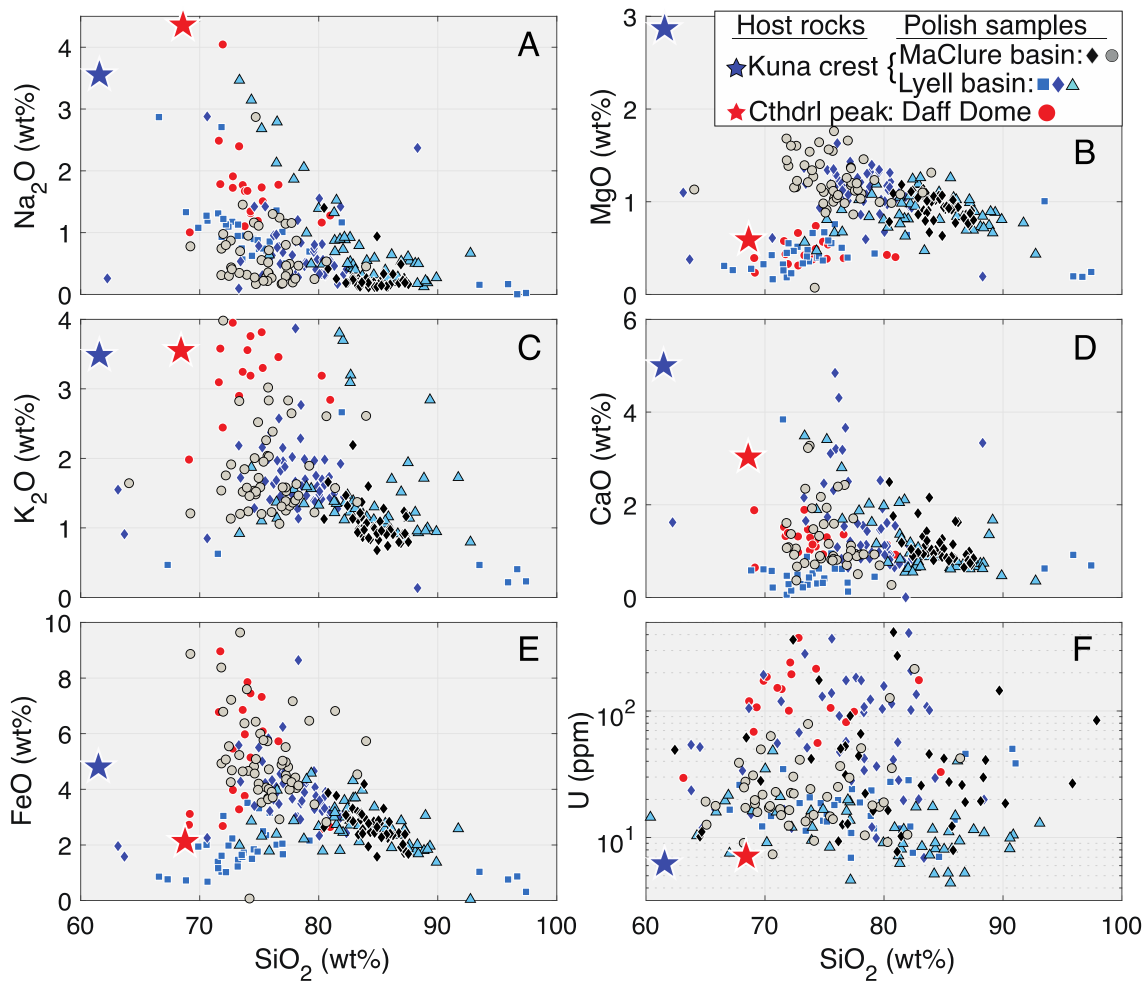
A
B
C
D
E
F
Host rocks
Polish samples
Kuna crest
MaClure basin:
Lyell basin:
Cthdrl peak: Daff Dome
Na2O (wt%)
MgO (wt%)
K2O (wt%)
CaO (wt%)
FeO (wt%)
U (ppm)
SiO2 (wt%)
SiO2 (wt%)

FIGURE 4:

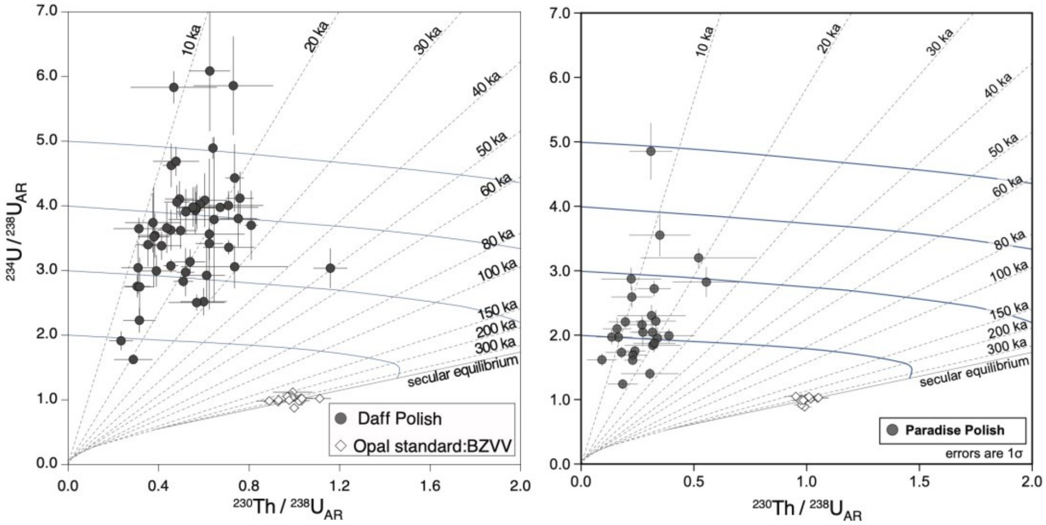

7.0
6.0
5.0
4.0
3.0
2.0
1.0
0.0
$^{234}U / ^{238}U_{AR}$
10 ka
20 ka
30 ka
40 ka
50 ka
60 ka
80 ka
100 ka
150 ka
200 ka
300 ka
secular equilibrium
Daff Polish
Opal standard:BZVV
0.0
0.4
0.8
1.2
1.6
2.0
$^{230}Th / ^{238}U_{AR}$
Paradise Polish
errors are 1σ
0.5
1.0
1.5